Efficient neutron production from sub-nanosecond laser pulse accelerating deuterons on target front side

D. Klir, J. Krasa, J. Cikhardt, R. Dudzak, E. Krousky, M. Pfeifer, K. Rezac, O. Sila, J. Skala, J. Ullschmied, and A. Velyhan

Citation: Physics of Plasmas **22**, 093117 (2015); doi: 10.1063/1.4931460
View online: http://dx.doi.org/10.1063/1.4931460
View Table of Contents: http://scitation.aip.org/content/aip/journal/pop/22/9?ver=pdfcov
Published by the AIP Publishing

Efficient neutron production from sub-nanosecond laser pulse accelerating deuterons on target front side

D. Klir,[1,2,3] J. Krasa,[3] J. Cikhardt,[1,2] R. Dudzak,[2,3] E. Krousky,[2,3] M. Pfeifer,[2,3] K. Rezac,[1,2] O. Sila,[1] J. Skala,[2,3] J. Ullschmied,[2,3] and A. Velyhan[3]
[1]*Faculty of Electrical Engineering, Czech Technical University in Prague, Technicka 2, 16627 Prague 6, Czech Republic*
[2]*Institute of Plasma Physics, ASCR, Za Slovankou 3, 182 00 Prague 8, Czech Republic*
[3]*Institute of Physics, ASCR, Na Slovance 2, 182 21 Prague 8, Czech Republic*

(Received 20 February 2015; accepted 7 September 2015; published online 22 September 2015)

Neutron-producing experiments have been carried out on the Prague Asterix Laser System. At the fundamental wavelength of 1.315 μm, the laser pulse of a 600 J energy and 300 ps duration was focused on a thick deuterated-polyethylene target. Neutron yields reached $(4.1 \pm 0.8) \times 10^8$ at the peak intensity of $\approx 3 \times 10^{16}$ W/cm^2. A more detailed analysis of neutron time-of-flight signals showed that a significant fraction of neutron yields was produced both by the ^{2}H(d,n)^{3}He reaction and by other neutron-producing reactions. Neutron energies together with delayed neutron and gamma emission showed that MeV deuterons escaped from a laser-produced plasma and interacted $\approx$50 ns later with a borosilicate blast-shield glass. In order to increase DD neutron yields and to characterize deuteron beams via nuclear reactions, a secondary deuterated polyethylene target was used in a pitcher-catcher scheme at the target front side. In this experimental arrangement, the neutron yield reached $(2.0 \pm 0.5) \times 10^9$ with the peak neutron fluence of $(2.5 \pm 0.5) \times 10^8$ n/sr. From the neutron yield, it was calculated that the secondary target was bombarded by 2×10^{14} deuterons in the 0.5–2.0 MeV energy range. The neutron yield of 2×10^9 at the laser energy of 600 J implied the production efficiency of 3×10^6 n/J. A very important result is that the efficient neutron production was achieved with the low contrast, sub-nanosecond laser pulse of the intensity of 10^{16} W/cm^2. The latter parameters can be achieved in a rep-rate mode more easily than ultra-high intensities and contrasts. © *2015 AIP Publishing LLC*. [http://dx.doi.org/10.1063/1.4931460]

I. INTRODUCTION

Neutron production during the laser interaction with deuterated targets has been studied intensively in connection with the controlled thermonuclear fusion research. The main idea of the thermonuclear mechanism is to initiate nuclear fusion reactions, and usually to generate fusion neutrons, with ions accelerated by elastic collisions inside high-temperature Maxwellian plasmas. To achieve sufficiently high temperatures, powerful laser systems with a high-energy beam are required. The first attempts to heat plasmas to keV temperatures were carried out shortly after the invention of a visible laser. As far as the first experiments focused on neutron production are concerned, mention should be made of irradiation of planar deuterated targets by the lasers with the beam energy of tens of Joules at the end of the 1960s.[1–5] The experiments continued with spherical compressions in the early 1970s (e.g., Ref. 6). From that time on, a significant progress in the inertial confinement fusion (ICF) has been made with both direct- and indirect-drive in the USA, the former Soviet Union, Russia, Japan, and France (cf. Ref. 7 and references therein). Recently, cryogenic DT layered capsules at the 2 MJ NIF facility have produced up to 10^{16} DT neutrons accompanied with the DD yields of the order of 10^{13} (Ref. 8).

Apart from the thermonuclear mechanism, DD or DT fusion neutrons can be produced by beam-target mechanism. In this case, the interaction of laser pulses with deuterated targets at relativistic intensities accelerates ions to MeV energies by strong electric fields. Then, accelerated ion beams may fuse with target ions. In the late 1990s, a significant number of non-thermal neutrons up to 7×10^7 n/sr were produced with sub-kilojoule chirped-pulse amplification glass laser systems irradiating solid deuterated-polyethylene targets.[9–12] A further progress in neutron production by lasers was associated with an increasing availability of repetitive tabletop Ti:sapphire lasers. The growing attention to neutron production was given by attractive applications of repetitive portable lasers in radiation material science, radiobiology, nuclear medicine, cargo inspection, or improvised explosive device detection. In order to obtain neutron numbers sufficient for these applications, various targets were tested. There have been many experiments focused on neutron production by intense lasers. In this paper, we restricted ourselves to experiments that are relevant to our work, namely, to irradiation of deuterated targets and to the beam-target production of neutrons. Besides solid-density deuterated targets[13,14] and heavy-water droplets,[15,16] the Coulomb explosion of deuterium[17–19] or deuterated-methane clusters[20] attracted the greatest interest. In the case of relativistic interaction with thin-foil targets, it has been found that intense ion beams can be accelerated on a target rear side by the target-normal sheath acceleration (TNSA) mechanism.[21,22] It was natural to employ these ions for more efficient neutron production by using a secondary target, i.e., a so-called pitcher-catcher scheme.[15,23] Within this scheme, there was a

possibility to explore a wider range of initial conditions. For instance, various nuclear reactions were researched with different targets (catchers).[24–26] Recently, intense lasers with ultrahigh contrasts have enabled efficient deuteron acceleration and high neutron yields through the break-out afterburner (BOA) mechanism.[27] Even more efficient neutron production is expected to be achieved with radiation pressure acceleration (RPA) of ions[28] at intensities above $10^{23}\,\mathrm{W/cm^2}$.

The neutron yields in the experiments mentioned above are displayed in Fig. 1. In the case of solid deuterated targets and femtosecond (black squares) or picosecond (red circles) lasers, it seems that the neutron yields for a specific target and laser pulse duration tend to increase with a higher intensity (see Fig. 1(a), cf. with Ref. 11). However, the relativistic intensities above $10^{18}\,\mathrm{W/cm^2}$ are not necessary to accelerate deuterons to fusion energies. In order to accelerate $>100\,\mathrm{keV}$ deuterons, the intensities of about $10^{16}\,\mathrm{W/cm^2}$ are sufficient.[49,50] From this point of view, the laser intensity is not the only parameter influencing the total neutron yield. As shown in Fig. 1(b), the neutron yield Y_n is strongly influenced also by the total energy of a laser beam E_laser. A good fit was found for a power-law dependence $Y_\mathrm{n} \propto E_\mathrm{laser}^{-(1.1\pm0.1)}$. Fairly high neutron yields were achieved during the interaction of kilojoule laser pulses at the intensities of $10^{16}\,\mathrm{W/cm^2}$. The research of neutron production at $10^{16}\,\mathrm{W/cm^2}$ intensities is important for several reasons. First, lower intensities are more suitable for rep-rate sub-kJ class laser technology that is now being developed for applications in industry and in research.[51] Second, the intensities of about $10^{16}\,\mathrm{W/cm^2}$ are relevant to the research of various shock-ignition schemes.[52] Third, at $\approx 10^{16}\,\mathrm{W/cm^2}$, the acceleration of deuterons at the front side of thick targets is not well understood. Since fusion neutrons are significantly influenced neither by electric nor by magnetic fields, diagnostics of neutrons might provide information about deuterons, and therefore it could provide a deeper insight into the process of deuteron acceleration. Whereas a large number of studies have been recently devoted to neutron production by ultra-intense lasers, the experimental details on beam-target neutron production at $10^{16}\,\mathrm{W/cm^2}$ intensities and nanosecond or sub-nanosecond pulse durations are rather rare. These were the main reasons why we decided to research DD neutron production at the Prague Asterix Laser System (PALS).[53]

The results from the first experiments with thick $(CD_2)_n$ targets were published in Refs. 48 and 54. In those experiments, the emphasis was put on the correlation of neutron emission with accelerated ion beams. In this paper, a more detailed analysis of neutron time-of-flight (ToF) signals is provided, and the contribution of various nuclear reactions is discussed. On the basis of our findings, the experiment has been optimized with respect to high neutron yields. In Section II, the laser system, an experimental arrangement, and diagnostics used in our experiment are described. Section III provides the most important experimental results with irradiated deuterated polyethylene targets. The emphasis is put on a so-called extended ToF method which helped us to identify the delayed neutron emission and the contribution of non-DD nuclear reactions. On the basis of several independent results, it is shown that MeV deuterons escaped from a laser-produced plasma and interacted ≈50 ns later with a borosilicate blast-shield glass. Section IV describes the experiments where a secondary target was used to study parameters of the escaping deuterons and to increase neutron yields. Neutron measurements with various pitcher-catcher schemes at the thick-target front side are presented. For the first time, the deuterated catcher was placed on the thick-target front side in the target-normal direction. This way, the highest neutron yields were achieved. The secondary targets enabled the discussion of the parameters of deuteron beams which is the subject of Section V. Finally, Section VI contains the overall conclusions.

II. EXPERIMENTAL SET-UP AND DIAGNOSTICS

A. Laser system

Neutron-producing experiments were carried out on the PALS at the Institute of Plasma Physics in Prague.[53] At the

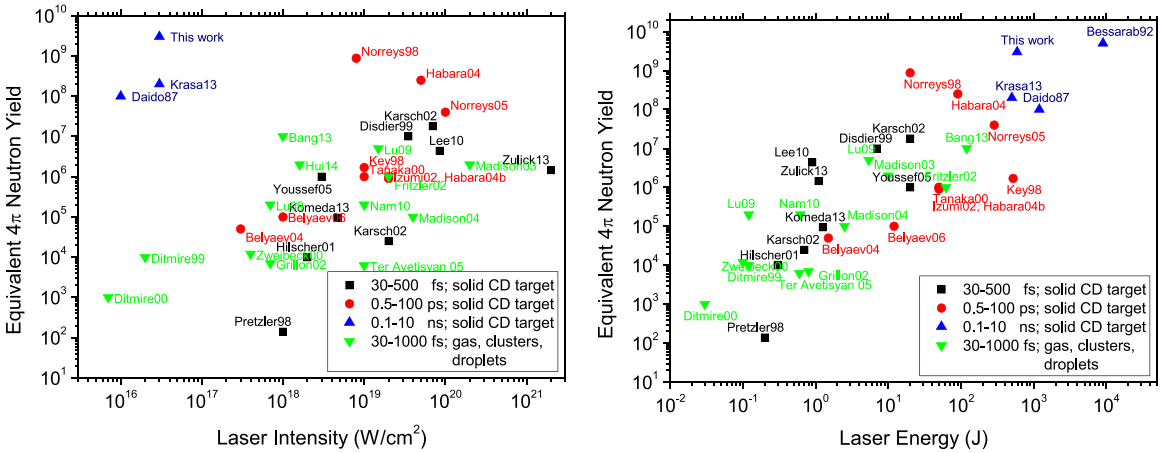

(a) Dependence of neutron yields on laser intensity

(b) Dependence of neutron yields on laser energy

FIG. 1. Neutron yields from deuterated targets irradiated by various laser systems. Data from Refs. 9, 10, 11, 12, 13, 14, 16, 17, 18, 19, 20, 26, 29, 30–33, 34, 35, 36, 37–39, 40, 41–45, 46, 47, and 48. ICF experiments and pitcher-catcher configurations with non-deuterated targets are not displayed. In the case of anisotropic neutron emission, equivalent 4π neutron yields were calculated from peak neutron fluences.

fundamental wavelength of $\lambda_L = 1.315\,\mu$m, the PALS laser was capable of delivering the pulse with a duration of 300 ps (FWHM) and an energy of ≈500 J on a target. Calculating with the waist of the focal spot of about 80 μm, a peak intensity of $I_L = 3 \times 10^{16}$ W/cm^2 and $I_L\lambda_L^2 = 4 \times 10^{16}$ (W/cm^2)μm^2 was obtained.

B. Experimental arrangement

The results presented in this paper were achieved in five independent experimental series of total 250 shots with deuterated-polyethylene targets. In most of the shots, the laser pulse was incident on planar targets at an angle of 0° from the target normal. The thickness of targets varied from 200 to 500 μm. The lens with a 593 mm focal length was protected with a borosilicate blast shield plate at 58 cm in front of targets. A schematic diagram of our experimental setup is depicted in Fig. 2.

C. Diagnostics

The interaction of the PALS laser system with deuterated targets was studied by ion and neutron diagnostics.

Parameters of ion emission were measured with the use of TasTrak CR-39 nuclear track detectors, ion collectors (ICs),[56] silicon-carbide (SiC) time-of-flight detector,[57] and a Thomson parabola spectrometer (TPS)[58] positioned in the far expansion zone, i.e., outside the recombination zone. The ion collector was screened with an Al foil of 6 μm in thickness to suppress generation of a photo-peak in the IC signal induced by extreme ultraviolet (XUV) radiation. The suppression of the photopeak of a 150 ns duration allowed us to detect MeV protons reaching the IC 50 ns after the laser pulse.[57] On the other hand, the 6 μm Al foil absorbed slower ions and, thus, limited the range of energy spectra to energies higher than 500 keV and 600 keV for protons and deuterons,

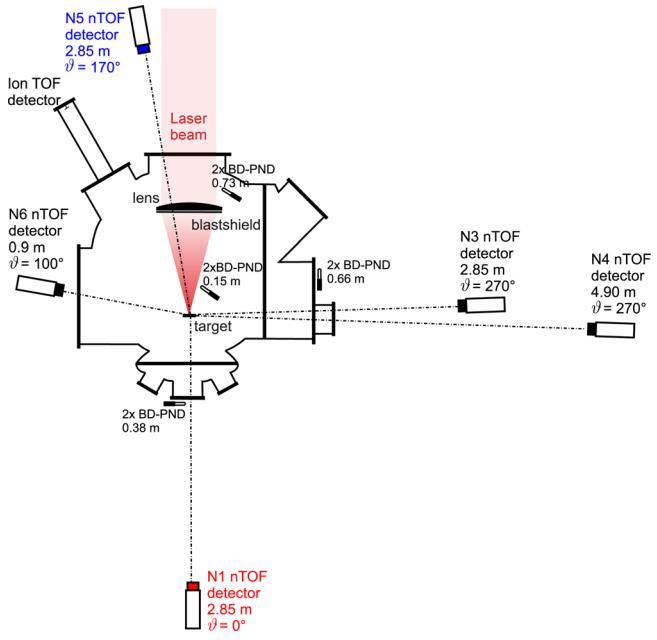

FIG. 2. Schematic diagram of a typical experimental setup and diagnostic tools, top view (not in scale).

respectively. The SiC detector also exhibited similar characteristics due to its internal structure, namely, 100 μm thickness of the epitaxial layer.[57]

The above-mentioned diagnostic tools were not able to distinguish deuterons from several other ion species. More specifically, distinguishing between deuterons and protons was the difficulty connected with CR-39 and ion ToF detectors. In the case of the Thomson parabola spectrometer with a microchannel plate, it was not possible to unambiguously distinguish deuterons from fully ionized carbon and oxygen ions because of the same charge-to-mass ratio. Therefore, in our experiments with deuterated targets, the emphasis was put on neutron diagnostics. Neutron fluence at various distances and directions was measured by the use of calibrated temperature-compensated bubble detectors–personal neutron dosimeters (BD-PNDs) with sensitivity of about 4 b/μSv.[59] Great attention was paid to the absolute calibration of BD-PNDs by our AmBe neutron source. A total neutron yield was calculated as an average from the neutron fluences detected by all BD-PNDs. Neutron energies and the time of neutron and high-energy bremsstrahlung (>1 MeV) emission were measured by 5 neutron ToF detectors. These detectors were composed of a NE102a equivalent fast plastic scintillator and a Hamamatsu photomultiplier (PMT) assembly.[60] The length of a plastic scintillator was 5 cm, whereas the effective cross-section was either 16 cm^2 or 350 cm^2. A temporal resolution of these neutron detectors operating in the current mode was about 5 ns. The neutron ToF detectors were placed in various directions at the distances between 90 and 490 cm from a target.

This set of diagnostic tools enabled us to obtain results, which are described in Sections III–IV. All times that are described in this paper refer to the peak of the laser pulse on a target ($t = 0$ ns).

III. LASER IRRADIATION OF A THICK $(CD_2)_n$ TARGET AT NORMAL INCIDENCE

A. Neutron yields

The interaction of the PALS laser system with a bulk deuterated polyethylene target produced neutron yields of the order of 10^8 at the laser energy of about 500 J. The neutron yield strongly depended on the focus position and varied from shot to shot. In the case of a target at (0 ± 100) μm from the focal spot, the average neutron yield was 10^8, whereas the peak neutron yield reached $(4.1 \pm 0.8) \times 10^8$ at the 650 J laser energy. These neutron numbers were sufficient to detect neutron time-of-flight signals with an acceptable signal-to-noise ratio on our detectors at a distance of up to 5 m.

B. High-energy bremsstrahlung radiation

The measurement of neutron time-of-flight signals was significantly influenced by preceding high-energy bremsstrahlung radiation. To prevent high-energy photons from saturating the photomultipliers, the detectors were shielded by interlocking lead bricks, and neutral density filters were placed between the scintillator and the PMT. Figure 3 shows

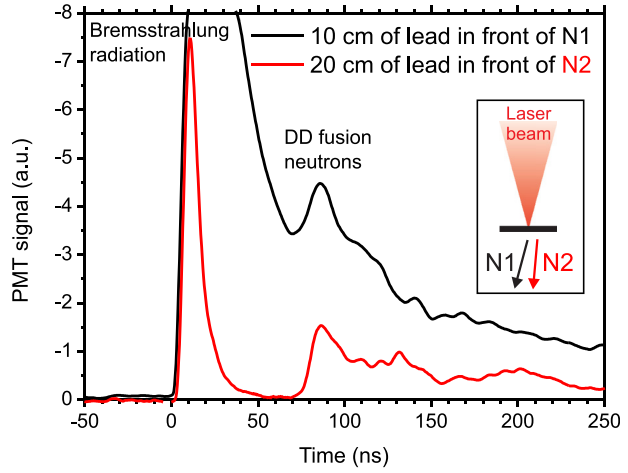

FIG. 3. Example of signals detected by the time-of-flight detectors with two different thicknesses of lead in front of the detectors. 5 cm lead bricks were placed around the detector. The detectors were located at the distance of 175 cm and 10° with respect to the incident laser beam. Shot no. 44417, neutron yield of 7×10^7.

an exemplary result recorded in the direction of laser beam propagation. Evidently, the 20 cm thickness of lead in front of the detector was needed to overcome the saturation in the forward direction. As for the radial direction, the 15 cm thickness of lead was sufficient. A negative effect of massive lead shielding is the significant scattering of 2.5 MeV neutrons. In the case of the 20 cm thickness, the instant neutron pulse is broadened to a 10 ns FWHM, and the peak is shifted by 4 ns.

The optimal thickness of the lead shielding was given by the energy and by the number of emitted photons. On the basis of the results with the shielding, we attempted to obtain more information about bremsstrahlung radiation in our experiment. The MCNP code[61] (F6 energy deposition tally) was therefore used to calculate the energy deposited by the incident photon in the scintillator behind lead shielding of various thickness. Fig. 4 shows the dependence of the deposited energy on the photon energy and on the thickness of the shielding in front of the detector.

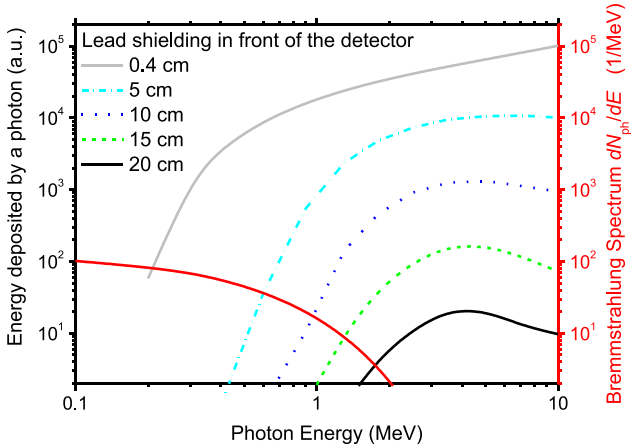

FIG. 4. Dependence of the energy deposited in the scintillator on photon energy. Note: The bremsstrahlung spectrum is represented by the solid red line with the red y-axis on the right.

Since the response of organic scintillators to photoelectrons is linear, the light output of the scintillator is proportional to the total deposited energy. Therefore, the large PMT signal behind 20 cm of lead (see Fig. 3) indicates that the laser interaction produced an abundance of photons with the >1.5 MeV energy. In order to obtain more details about bremsstrahlung spectra, we cross-calibrated three detectors with the same shielding. Then, it was possible to apply the Ross-filter method to the 0.2–2.0 MeV region. We observed the PMT signals behind lead shielding of various thickness, namely, of 0.4 cm, 5 cm, and 20 cm. In each shot, the ratios between signals at three cross-calibrated detectors were obtained. In high neutron yield shots, the 5-to-0.5 cm and 20-to-0.5 cm ratios were about 4×10^{-2} and 2×10^{-5}, respectively. These experimentally observed ratios were compared with the values calculated from the convolution of the energy-dependent deposited energy in Fig. 4 with the bremsstrahlung spectrum in the form of $dN_{ph}/dE \propto \exp(-\frac{E}{kT})$. A good fit of the experimentally observed ratios was found for the x-ray bremsstrahlung spectral temperature $kT \approx 500$ keV.

C. Neutron time-of-flight signals

The neutron-producing experiments at the Prague Asterix Laser System showed that neutron time-of-flight signals strongly depended on the total neutron yield. Therefore, the following experimental data will be presented according to the neutron yield. The data from lower-yield shots are presented first.

1. Lower neutron yields

An illustrative example of neutron time-of-flight signals detected in the shot with a lower neutron yield can be seen in Fig. 5. In this shot, the total yield was 10^7 neutrons. As shown in Fig. 5, the neutron peak at 114 ns is very close to the time-of-flight of 2.5 MeV neutrons. If we assume that

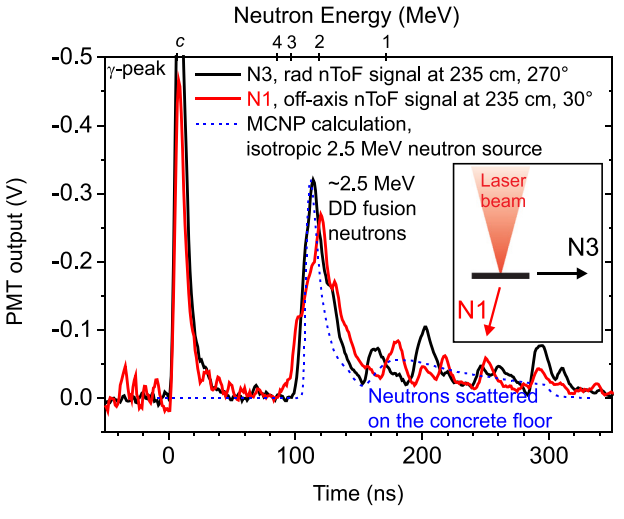

FIG. 5. Signals recorded by the nToF detectors at 235 cm and at two different angles with respect to the incident laser beam. 20 cm of lead was used in front of the detectors. The MCNP calculation included an isotropic 2.5 MeV neutron source, the simplified model of the experimental chamber, a concrete floor, and the lead shielding of the detector. Shot no. 44449, neutron yield of 10^7.

neutrons are produced at the irradiated target simultaneously with the laser pulse interaction, the arrival time of 2.5 MeV neutrons at the detector at 235 cm is 109 ns. The observed difference between 114 and 109 ns can be explained by neutron scattering on the lead shielding and other experimental hardware (see the result of the MCNP calculation in Fig. 5). The neutron emission seemed to be isotropic. However, detailed analysis could not be made due to a small number of neutrons detected by scintillators with a small detection area. In the case of the scintillator with the effective cross-section of 16 cm^2, the neutron yield of 10^7 implies that only 200 neutrons can be registered at the distance of 235 cm. Taking into account also the detection efficiency and the signal reduction due to neutron scattering, it follows that the shot noise strongly influenced nToF signals in low-yield shots. As a result, we decided to perform a more detailed neutron time-of-flight analysis by using a distant detector with a larger scintillator. For this purpose, a scintillator with a 350 cm^2 effective cross-section was placed at about 490 cm from the source. The obtained neutron spectrum viewed radially can be seen in Fig. 6. Neutron spectra similar to that displayed in Fig. 6 were observed also in other directions. Most of the neutrons were produced with the energy between 2.2 and 3.0 MeV. Therefore, on the basis of the kinematics of the DD reaction,[55] it is possible to conclude that the neutron production in lower-yield shots was caused by deuterons with kinetic energies of the order of 100 keV.

2. Higher neutron yields

Qualitatively different neutron time-of-flight signals were observed in the shots with $>10^8$ neutrons. Fig. 7 shows typical waveforms recorded by three nToF detectors at about 280 cm from the irradiated target. In all high-yield shots, neutrons were detected first in the backward direction with respect to the incident laser beam (cf. Fig. 7). It is a significant result since the fastest neutrons have not been observed in the backward direction in other experiments displayed in Fig. 1. As shown in Fig. 7, other characteristic features of

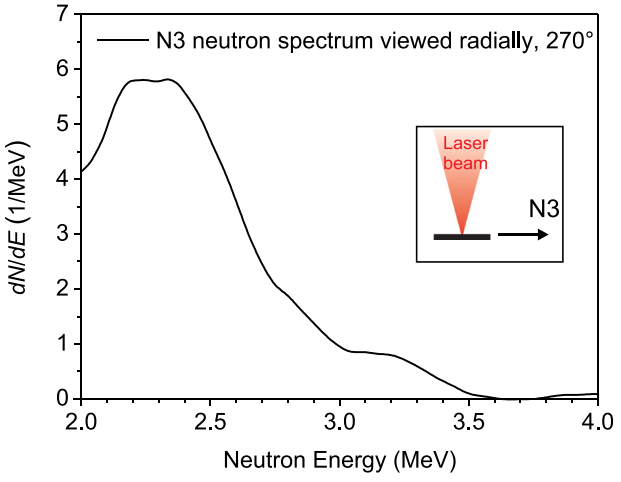

FIG. 6. Time-integrated neutron energy distribution function $f(E, \phi, \vartheta) = dN/dE$ in the radial direction ($\vartheta = 270°$) calculated from the nToF detector at 490 cm. Shot no. 46586, neutron yield of $(1.7 \pm 0.3) \times 10^7$. Note: The dependence of the detector sensitivity on a neutron energy is not taken into account.

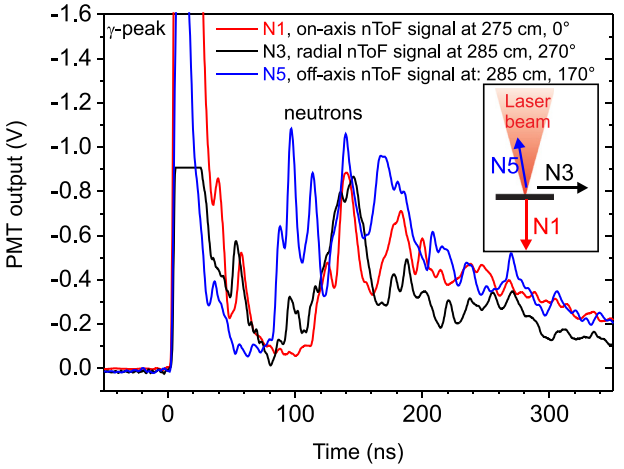

FIG. 7. Signals recorded by the time-of-flight detectors at about 280 cm in three different directions with respect to the incident laser beam. Shot no. 46576, neutron yield of $(3.0 \pm 0.5) \times 10^8$.

higher-yield shots were anisotropic neutron emission and longer ToF signals consisting of several neutron peaks. Unlike lower-yield shots, these peaks cannot be explained by the kinematics of the DD reaction, neutron scattering, and/or by shot-noise only. In order to explain the observed signals, we were interested in other neutron-producing reactions. Due to the composition of our $(CD_2)_n$ targets, it was natural to seek the contribution of the $^{12}C(d,n)$ and $^{2}H(c,n)$ reactions.[38,47,62,63] On the one hand, the tail of neutron signals could be formed by less energetic neutrons from the latter endoergic reactions. On the other hand, however, the contribution of these reactions would significantly prevail over the $^{2}H(d,n)$ reaction only if a deuteron energy is higher than 2 MeV. At the PALS facility, these deuterons are not numerous and, consequently, deuterated polyethylene targets should produce mainly DD neutrons.

As a result, we were looking for other interpretations of the observed signals. For instance, the long tail of ToF signals could have been caused by delayed neutron emission. From this point of view, it seemed useful to study the duration of neutron emission by placing one radial neutron ToF detector as close to the irradiated target as possible. Initially, we expected that narrow ToF signals would be recorded. Surprisingly, the width of neutron signals at 90 cm was typically 100 ns (FWHM). Results from 8 low- and high-yield shots are displayed in Fig. 8.

In Fig. 8, the peak at 45 ns corresponded to 2.5 MeV neutrons produced during or shortly after the laser pulse interaction with a polyethylene target. However, an intense neutron signal was also observed between 60 and 120 ns. The late neutron signal was dominant particularly in high-yield shots (see, e.g., shot No. 44491 in Fig. 8). The high ratio between the second and the first pulse could not be explained by nuclear reactions of deuterons with carbon ions and/or by neutron scattering. Instead of it, the ToF signals in Fig. 8 suggested a secondary source of neutrons with a delayed emission. Since a majority of energetic deuterons were emitted towards the blast shield protecting the lens, there was a possibility of nuclear reactions induced by fast deuterons hitting the borosilicate glass (see Fig. 2).

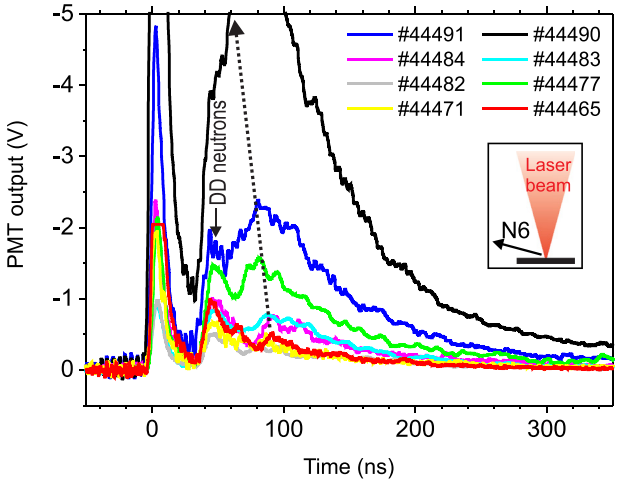

FIG. 8. Signals recorded by the radial time-of-flight detector at 90 cm in 8 shots. The relative scale of the y-axis is the same for all waveforms. The neutron yield ranges from 4×10^6 to 2×10^8. As indicated with a dashed arrow, the delay of the late emission was decreasing with an increasing neutron yield.

D. Neutrons from the deuteron bombardment of the borosilicate blast-shield glass

Neutrons produced in the borosilicate glass can be distinguished by two characteristic features. The first attribute of neutrons originating from the borosilicate glass is a neutron energy spectrum, which differs from that of the ^{2}H(d,n)^{3}He reaction. The second feature is a delay in the production of neutrons. If the neutron production exhibits the delay after the laser pulse interaction with a target, a standard ToF method with one detector is not sufficient to characterize a neutron source. The arrival time of a neutron to a detector is given by the time of neutron production and by a neutron velocity. In order to distinguish neutron production time from a neutron energy spectrum in ToF signals, several neutron ToF detectors should be placed in one direction at different distances (so-called extended time-of-flight method[55]). For this reason, we placed two detectors in the radial direction at both 287 cm and 490 cm from the target. It should be noted that the distance of the detector from the target was approximately the same as the distance from the center of the glass. Typical ToF signals are displayed in Fig. 9.

The first unambiguous result of the extended ToF method is the energy of the fastest neutrons. The energy of the fastest neutrons can be calculated from the onsets of neutron signals t_1, t_2 measured at two distances l_1, l_2, respectively. The lower bound of the highest velocity is estimated as $v_n = (l_2 - l_1)/(t_2 - t_1)$. Calculating with the onsets displayed in Fig. 9, the highest neutron energy was above 13 ± 1 MeV. The maximum kinetic energies of deuterons measured by ion ToF detectors were about 2 MeV; therefore, the >13 MeV neutrons had to be produced by a nuclear reaction with the Q-value higher than 10 MeV. Such exoergic reactions are not numerous. Since the borosilicate blast shield contains boron atoms, one of the most reasonable candidates is the ^{11}B(d,n) reaction with $Q = 13.73$ MeV and with a high cross-section above a 1 MeV deuteron energy.

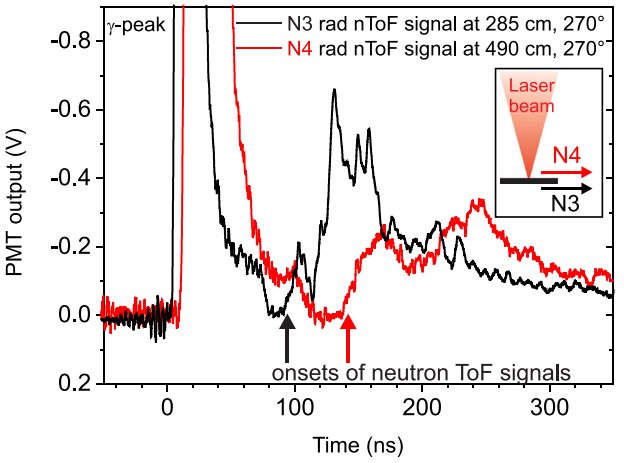

FIG. 9. Time-of-flight signals recorded by the radial detectors at 287 cm and at 490 cm from the target. Shot no. 46567, neutron yield of $(0.9 \pm 0.3) \times 10^8$.

In order to confirm the hypothesis of the borosilicate glass as a neutron source, it is possible to calculate the time when the fastest neutrons were produced. From the onsets in Fig. 9, we calculate that the production time of the fastest neutrons was $t_0 = t_1 - l_1(t_2 - t_1)/(l_2 - l_1) = 44 \pm 4$ ns after the laser pulse interaction. This production time corresponded to the time-of-flight of 1.8 ± 0.3 MeV deuterons from the irradiated target to the borosilicate glass. The deuteron energy of 1.8 MeV is quite reasonable because a similar value was measured by our silicon-carbide ToF detector. This detector recorded the fastest deuterons with the kinetic energy of about 1.5 MeV in this particular shot no. 46567 (cf. the dashed line in Fig. 10(a)).

The production time and energies of the fastest neutrons are not the only indications of neutrons generated in the borosilicate glass. The delayed production of energetic neutrons in the blast shield could also explain the neutron peaks detected between 60 and 100 ns in Fig. 8, the multi-peak structure of ToF signals in Fig. 7, as well as higher neutron fluence observed by the BD-PND detectors close to the blast shield. (We note that a different position of the secondary neutron source was taken into account when evaluating total neutron yields.) Besides these observations, we were searching for more direct signs of the B(d,n) reactions in neutron ToF signals.

As was mentioned above, >13 MeV neutrons could be produced by the ^{11}B(d,n)^{12}C reaction with the Q-value of 13.73 MeV. However, the residual carbon nuclei often remain in excited states ($E_1 = 4.44$ MeV, $E_2 = 7.66$ MeV, and $E_3 = 9.64$ MeV), and therefore several neutron groups are emitted.[64,65] In particular, the excited levels E_1 and E_3 are significant. One also has to take into account that the borosilicate glass does not contain only a fraction (5%–6%) of ^{11}B isotopes but also a small (1%–2%) fraction of ^{10}B isotopes. Neutrons can be therefore produced by the ^{10}B(d,n)^{11}C reaction, which has the Q-value of 6.47 MeV and a high cross-section for >500 keV deuterons. As a result, the borosilicate glass might produce a large number of neutron groups, which are broadened due to a wide energy spectrum of deuterons slowing down inside the glass. At our nToF detectors, these broad neutron groups overlapped due

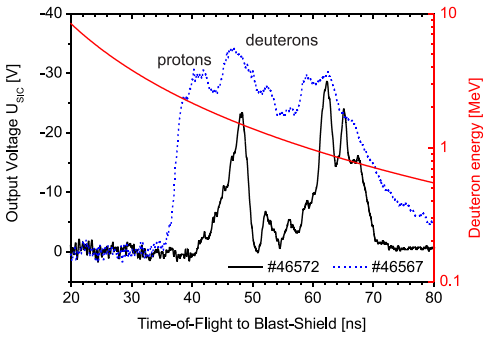

(a)Ion ToF signals (black and blue) measured by the silicon carbide detector at 150 degrees in shot no. 46567 and no. 46572 (recalculated for the blast shield at 58 cm). A 6 μm aluminum foil was used to filter x-rays. Note: The signals from SiC detectors agreed with ion collector signals.

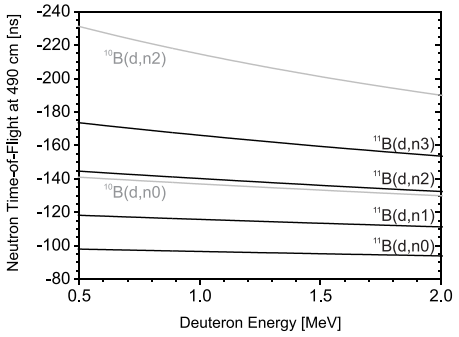

(b)Deuteron-energy dependence of neutron time-of-flight from the blast shield to the radial detector at 490 cm.

FIG. 10. Shot no. 46572, neutron yield of $(0.8 \pm 0.2) \times 10^8$. Shot no. 46567, neutron yield of $(0.9 \pm 0.3) \times 10^8$.

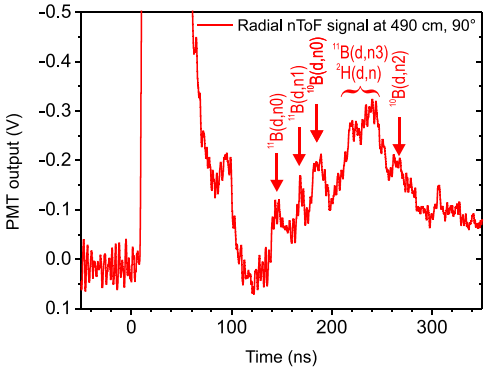

(c)Neutron ToF signal recorded by the radial detector at 490 cm from the target in shot no. 46572.

to a long neutron emission from the glass. The long duration of neutron emission was caused by various time-of-flights of deuterons from the irradiated target to the blast shield. Despite all these effects, various neutron groups were recognized in shots with moderate deuteron energies as shown in Fig. 10.

Fig. 10(a) shows the ion TOF signal recalculated for the distance of the borosilicate blast shield. In shot no. 46572, deuteron energies exceeded 1 MeV and the neutron-producing deuterons were striking the blast shield between 50 and 70 ns. The time-of-flight of various neutron groups from the blast shield to the radial detector is displayed in Fig. 10(b). On the basis of Figs. 10(a) and 10(b), several neutron groups were identified in the neutron ToF signal in Fig. 10(c). (When evaluating the contribution of various neutron groups, the fact that the spectral response of the detector is increasing with a neutron energy has to be taken into account. Namely, a >10 MeV neutron from the B(d,n) reaction produces higher light outputs than a 2.5 MeV neutron.)

The neutron groups from the B(d,n) reactions were identified most easily in the radial direction. Nevertheless, they were observed also in other directions. In higher-yield shots (e.g., in the shot displayed Fig. 9), the fastest neutrons up to 16.0 ± 0.5 MeV were observed in the backward direction with respect to the incident laser beam, i.e., in the direction in which deuteron beams stroked the blast shield. The 16 MeV neutrons could be produced by 2.5 MeV deuterons. This result is an important confirmation of >2 MeV deuterons in our experiment, since it is difficult to distinguish the fastest deuterons from protons with our ion ToF detectors and CR-39 nuclear track detectors. An important implication of the occurrence of 2.5-MeV deuterons is a contribution of

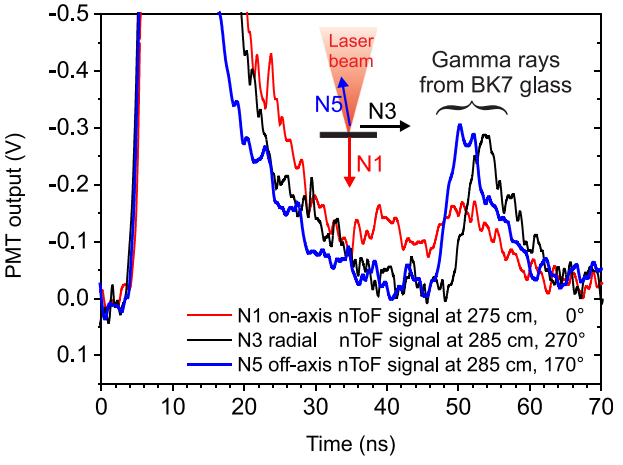

FIG. 11. Gamma-rays recorded by the time-of-flight detectors at about 280 cm from the target. Shot no. 46580, neutron yield of $(1.2 \pm 0.3) \times 10^8$.

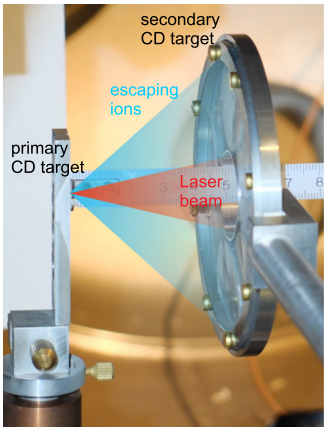

(a)Pitcher-catcher target scheme at the normal incidence of the laser beam on the primary target. The secondary target was on the front side, at 5 cm from the irradiated target.

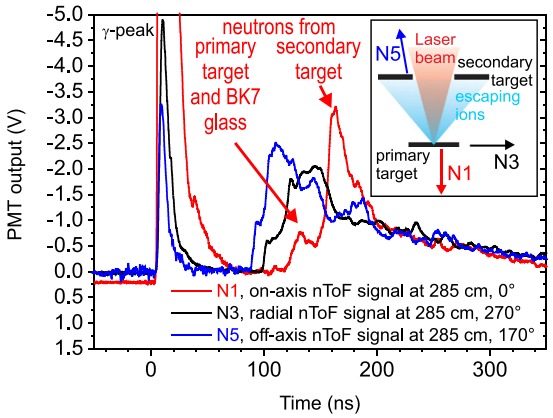

(b)Signals recorded by the time-of-flight detectors at about 280 cm from the primary target and at three different angles with respect to the incident laser beam.

FIG. 12. Shot no. 46609, neutron yield of $(5.3 \pm 1.0) \times 10^8$. Note: A fraction of neutrons was still produced in the borosilicate glass.

the $^{16}O(d,n)^{17}F$ reaction inside the borosilicate glass. This reaction has the threshold at 1.83 MeV but the cross-section approaches 200 mb for 2.5-MeV deuterons.

The last experimental evidence of deuterons striking the borosilicate glass was gamma-ray radiation observed at about 50 ns after the laser pulse interaction. These gamma-rays were likely produced during the fast transition of the excited ^{12}C and ^{11}C isotopes to their ground states. An indication of these gamma rays was recorded at 55 ns in the shot displayed in Fig. 7. A more illustrative example can be seen in Fig. 11 where three ToF signals are displayed.

IV. NEUTRON PRODUCTION FROM A PITCHER-CATCHER SCHEME AT THE TARGET FRONT SIDE

In Section III, we presented the experimental results which were obtained during the irradiation of a deuterated polyethylene target by the PALS laser. It has been observed that high-yield shots were accompanied by 13 MeV neutrons, the delayed emission of neutrons and gamma-rays, higher fluences of neutrons near the blast-shield glass, and by the neutron groups which are specific for the B(d,n) reactions. These observations could be explained by fast deuterons escaping laser-produced plasmas and interacting ≈50 ns later with the borosilicate blast-shield glass. Since the concentration of boron atoms in the glass is low and the stopping power of ions is relatively high, it seems natural to use a converter that is more efficient than our borosilicate glass. In order to increase neutron yields and to study parameters of deuteron beams, we decided to use a secondary target in three different pitcher-catcher target schemes. The results from these experiments are described in Sections IV A–IV C.

A. Normal incidence of the laser beam on the primary target

In our first pitcher-catcher target setup, the laser pulse was incident on the primary deuterated target identically to the shots presented above, i.e., at the normal incidence. In order to "catch" deuterons escaping the primary target from the front side, the secondary deuterated polyethylene target of a 300 μm thickness was placed off-axis at an angle of 20°–40° with respect to the target normal (cf. the scheme in Fig. 12(a)). The 50 cm^2 active area of the secondary target at a 6 cm distance represented a solid angle of about 1.4 sr.

Using this secondary target, the total neutron yields were quite reproducible and varied between 5×10^8 and 6×10^8 per one shot. The exemplary nToF signals are displayed in Fig. 12(b). As shown in Fig. 12(b), most of the neutrons were produced by the "catcher." For the interpretation of nTOF signals, the on-axis detector in the direction of the laser beam proved to be very useful. It follows from the kinematics of the DD reaction that the slowest neutrons from the secondary target were produced backward with respect to the deuteron beam, i.e., in the direction of the laser beam. Taking into account also the time-of-flight of ions from the irradiated target to the catcher, neutrons from the primary and secondary targets could be easily distinguished at the on-axis detector N1. At this ToF detector, the peak of DD neutrons with a 1.8-MeV energy was observed. In contrast, the main neutron pulse at the off-axis detector (N5) was formed by ≈3.8 MeV neutrons. Calculating with these energies, it can be inferred that the main neutron peak was produced by deuterons with the effective energy of about 0.8 MeV.

B. 30° incidence angle of the laser beam on the target

In the case of the normal incidence of the laser beam on the primary target, it was not possible to place the secondary target on-axis, since it would have interfered with the focused laser beam (see Fig. 12(a)). Therefore, we decided to test another experimental arrangement. In that arrangement, we set the incidence angle of the laser beam on the target surface to 30°. The secondary deuterated target was placed in the target-normal direction at about 14 cm from the irradiated primary target. We used the same secondary target as shown in Fig. 12(a). The only difference was that the entrance hole for the laser beam was filled with a thick deuterated polyethylene foil. Then, the 60 cm^2 active area of the secondary target represented a solid angle of about 0.4 sr. In

the target-normal direction, a large number of accelerated deuterons could be used to increase neutron yields. Indeed, the peak neutron yield in this experimental arrangement reached $(2.0 \pm 0.5) \times 10^9$. The neutron emission was anisotropic with the peak fluence of $(2.5 \pm 0.5) \times 10^8$ n/sr in the direction in which deuterons bombarded the secondary target. In a perpendicular direction, the measured fluence was $(0.9 \pm 0.3) \times 10^8$ n/sr. A large number of nuclear reactions inside the catcher target were verified by the post-shot gamma spectroscopy. By means of the NaI:Tl scintillation detector, we measured the ≈10 kBq positron activity of ^{13}N isotopes produced by the ^{12}C(d,n)^{13}N reactions in the polyethylene catcher.

C. High-energy neutrons from a LiF catcher

A pitcher-catcher target scheme can be used not only to increase neutron yields but also to produce high-energy neutrons. As mentioned above, we identified high-energy neutrons from the B(d,n) reactions in our TOF signals. In order to produce a higher number of more energetic neutrons, it seemed natural to employ the ^{7}Li(d,n) reaction ($Q = 15.03$ MeV). For this purpose, we placed a 17 cm^2 slab of a 1 mm thick LiF target at 10 cm from the primary $(CD)_n$ target. Experimental results obtained with this catcher were described in a detail in Ref. 66. At this point, we compare shots with and without the LiF catcher.

In Fig. 13, the radial nToF signals clearly show that the LiF catcher produced faster neutrons. The peak at 60 ns corresponded to 11 MeV neutrons from the LiF catcher. This neutron group originated from the ^{7}Li(d,n)^{8}Be reaction where the residual nuclei remained in the first excited state with $E_1 = 3.03$ MeV and $\Delta E_1 = 1.51$ MeV. Since the residual nuclei of this reaction often remain in excited states and three-body processes, namely, ^{7}Li(d,n + α)^{4}He, contribute to neutron production, >10 MeV neutrons formed only a quarter of the neutron yield produced by the LiF target.[67,68]

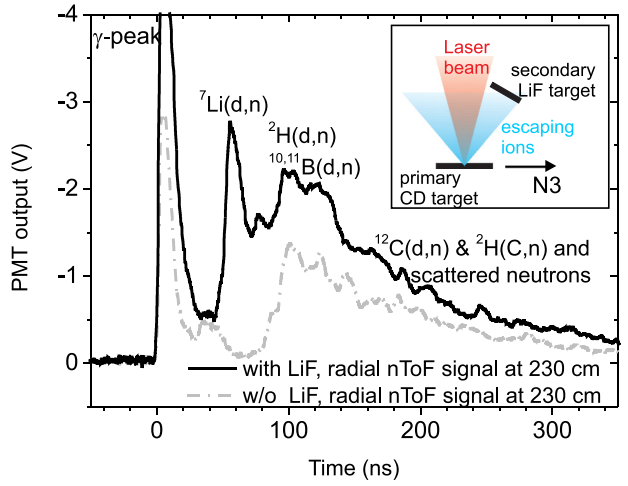

FIG. 13. Signals recorded by the radial time-of-flight detector N3 at about 230 cm from the irradiated target. Shot no. 44511 with the LiF slab (black line), neutron yield of $(3.4 \pm 0.7) \times 10^8$. Shot no. 44424 without the LiF slab (grey line), neutron yield of $(1.6 \pm 0.3) \times 10^8$.

V. DISCUSSION

At present, the interaction of ultra-short laser pulses with targets makes it possible to accelerate protons and deuterons to multi-MeV energies. This fact is used to produce fast neutrons by beam-target mechanism. In order to achieve high neutron yields, various neutron-producing reactions have been studied. The DD reaction is used quite often because this reaction has ≈100 mb cross-section and deuterated targets can be easily obtained and handled. The peak fusion cross-section is reached at a 2-MeV deuteron energy, but the cross-section is significant, i.e., above 25 mb, even for deuterons with a 150-keV energy. To accelerate hydrogen ions to >150 keV energies, the laser intensity of about 10^{16} W/cm^2 is sufficient. In Sections III–IV, we presented the experimental results that were achieved at the PALS facility with the peak intensity of 3×10^{16} W/cm^2. As shown in Figs. 5 and 6, the DD neutrons were clearly identified in the ToF signals. However, in the high-yield shots, the neutron spectra indicated that more neutron-producing reactions had to be taken into account.

In Section III, we showed that the properties of the PALS laser beam had also a positive effect on both hot electrons and fast deuterons. As far as hot electrons are concerned, the bremsstrahlung spectral temperature of 500 keV was inferred from the light outputs of the scintillators shielded by various thickness of lead. As for hydrogen ions, the energies up to 2 MeV were inferred from the Thomson parabola spectrometer, ion collectors, and CR-39 nuclear track detectors. On the one hand, the deuteron energy of 2 MeV is below the deuteron breakup threshold. On the other hand, however, 2-MeV deuterons might produce a large number of neutrons via deuteron stripping (d,n) reactions in various low-Z materials inside the experimental chamber. Besides the ^{12}C(d,n) reactions, the interaction of deuterons with boron atoms was identified in our time-of-flight signals (see Fig. 10). The B(d,n) reactions were generated during the bombardment of the borosilicate blast-shield glass by accelerated deuterons. Due to the low concentration of boron atoms in the borosilicate glass, it seemed natural to produce neutrons by a more efficient converter. For this purpose, we placed the secondary target at the primary-target front side in so-called pitcher-catcher scheme. The neutron-producing "catcher" was used to study the properties of accelerated deuterons, to change neutron emission spectra, and to increase neutron yields. These three applications of the catcher are discussed further below.

First, the neutron production from a secondary target provides important information about ions escaping the irradiated target. Ion beams at the PALS facility were diagnosed by several techniques. The advantage of the diagnostics based on nuclear reactions was that it enabled us to distinguish fast deuterons from protons. For instance, it was possible to estimate the number of deuterons interacting with the deuterated polyethylene catcher. On the basis of our ion and neutron measurements, we concluded that most of the neutrons originated from the secondary deuterated polyethylene target. Neutrons were produced mainly by deuterons in the 0.5–2.0 MeV energy range. In the high-yield shots, the mean

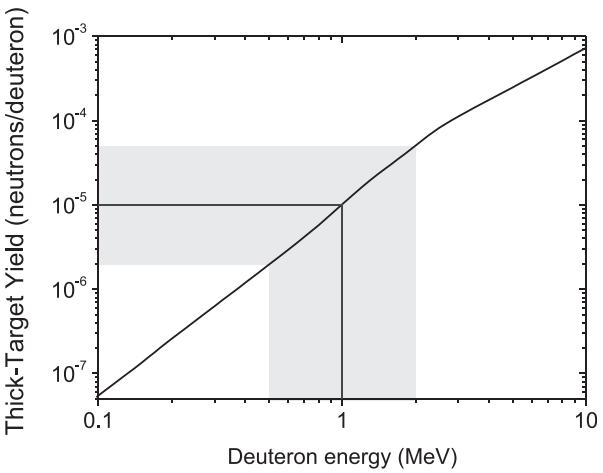

FIG. 14. Thick-target yield from $(CD_2)_n$ target calculated from ENDF and SRIM databases[67,69] using the procedure described in Ref. 70.

energy of neutron-producing deuterons was ≈1 MeV. At the deuteron energy of 1 MeV, the thick-target neutron yield from deuterated polyethylene is 10^{-5} (see Fig. 14). It means that 2×10^{14} deuterons were required to produce our peak neutron yield of about 2×10^9. 2×10^{14} deuterons with ≈1 MeV energy carried the total energy of 30 J. This energy represents 5% conversion efficiency of the 600 J laser beam to fast deuterons.

Second, in order to change neutron spectra, we decided to use the ^{7}Li(d,n) reaction, and we placed a 1 mm thick LiF target in the path of accelerated deuterons. Even though our LiF target covered a small solid angle of about 0.15 sr and it was not placed in the target normal direction, a significant increase of 10-MeV neutrons was recorded by the ToF signals as shown in Fig. 13.

Third, to increase the total neutron yield, we used large deuterated polyethylene targets that covered a greater solid angle. In several shots, we turned the irradiated deuterated target by 30°. Then, it was possible to place the "catcher" in the target-normal direction. This way the PALS laser generated 2×10^9 neutrons originating mostly from the DD reaction. According to our best knowledge, it is the highest DD neutron yield produced by a sub-kilojoule laser (see Fig. 1). A higher DD neutron yield of 5×10^9 was achieved during the irradiation of a spherical deuterated target with the 12 beam, 12 kJ ISKRA-5 laser system.[33] An even higher number of DD neutrons were produced by the thermonuclear mechanism when a cryogenic deuterium target was heated and compressed by powerful laser systems, such as Omega[71] or NIF.[8]

At this point, it seems interesting to calculate the neutron production efficiency in terms of number of neutrons per one joule of laser beam energy. In our experiment, the DD neutron yield of $(2.0 \pm 0.5) \times 10^9$ was achieved with the laser beam energy of about 590 J. It means that the neutron production efficiency reached 3.4×10^6 n/J. This value agrees with the energy-dependent DD neutron production efficiency of optimized plasma-based devices (see Fig. 11 in Ref. 72). In Ref. 72, it has been shown that the efficiency is rising with an increasing energy input into plasmas regardless the type of a plasma device. In order to generate neutrons with a high wall-plug efficiency, efficient conversion of stored electrical energy into plasmas is required. From this point of view, a high (10%) conversion efficiency of z-pinches seemed to be very promising.[72–74] Nevertheless, a similar conversion efficiency can be achieved with newly developed diode-pumped lasers. Therefore, the recent advance in laser technology might enable the construction of versatile laser-based neutron sources that are suitable for many applications in near future.

VI. CONCLUSIONS

The interaction of the 600 J, 300 ps laser pulse with bulk deuterated polyethylene targets was studied at the PALS facility. The long laser-pulse was observed to accelerate not only a large number of protons but also heavier ions such as deuterons. Neutron yields reached $(4.1 \pm 0.8) \times 10^8$ at the peak intensity of 3×10^{16} W/cm^2. A more detailed analysis of neutron time-of-flight signals showed that a significant fraction of neutron yields was not produced by the ^{2}H(d,n)^{3}He reaction. It was confirmed that a large number of >500 keV deuterons escaped laser-produced plasmas and interacted with the material inside the experimental chamber. In order to increase neutron yields and to study the parameters of deuteron beams, the secondary deuterated polyethylene target was used in the pitcher-catcher scheme at the target front side. In this experimental arrangement, the neutron yield reached $(2.0 \pm 0.5) \times 10^9$. From the neutron yield, it was calculated that the secondary target was bombarded by 2×10^{14} deuterons in the 0.5–2.0 MeV energy range. The total beam energy of 30 J represented 5% conversion efficiency of the 600 J laser beam to fast deuterons.

The neutron yield of 2×10^9 at the laser energy of 600 J implied the production efficiency of 3×10^6 n/J. The high efficiency of fast deuteron and neutron production is important for future applications of lasers. A very important result of our experiments is that the efficient neutron production was achieved with the low contrast (10^{-6}), sub-nanosecond laser pulse of the intensity of 10^{16} W/cm^2. The latter parameters can be achieved in a rep-rate mode more easily and cheaply than 10^{20} W/cm^2 intensities and high contrasts. Low contrast, sub-nanosecond pulses usually do not require beam transport in vacuum and sophisticated laser technology including pulse compressors or plasma mirrors. A larger spot size can be achieved with a parabolic mirror or lens being placed far enough from an irradiated target. This way, the influence of target debris can be mitigated.

Finally, one improvement of our experimental setup should be mentioned. In our pitcher-catcher scheme, the relatively large secondary target was placed at about 10 cm from the primary target. On the one hand, it was possible to use the catcher in many shots. On the other hand, the spatial region of neutron production was quite extensive. Therefore, a more compact scheme should be tested. Moreover, if a secondary target is ionized by x-rays, or by the second laser beam, the stopping power of deuterons in a secondary target might be reduced. This would lead to a further increase of

neutron production efficiency, which could be sufficient for applications of lasers as compact neutron sources. In order to find the optimal conditions for the highest neutron yields, the properties of ion acceleration mechanisms have to be taken into account. Since ion acceleration mechanisms at target front side are not fully understood,[36,75–77] a more detail research of these mechanisms will be the subject of further experiments at the PALS facility.

ACKNOWLEDGMENTS

The authors gratefully acknowledge the support of the staff of the PALS laser facility without whose assistance this work would not have been possible. This research has been supported by the Grant Agency of the Czech Republic (Grant No. P205/12/0454), the Czech Ministry of Education (Grant Nos. LD14089, LG13029, LH13283, and LM2010014), the IAEA (Grant No. RC17088), and the CTU (Grant No. SGS 10/266/OHK3/3T/13). This product is co-financed by the European Social Fund and the state budget of the Czech Republic (Project No. CZ.1.07/2.3.00/20.02.0079).

[1]N. G. Basov, S. D. Zakharov, P. G. Kryukov, Yu. V. Sendetskii, and S. V. Chekalin, JETP Lett. **8**, 14–17 (1968).
[2]F. Floux, D. Cognard, L.-G. Denoeud, G. Piar, D. Parisot, J. L. Bobin, F. Delobeau, and C. Fauquignon, Phys. Rev. A **1**, 821 (1970).
[3]J. W. Shearer, S. W. Mead, J. Petruzzi, F. Rainer, J. E. Swain, and C. E. Violet, Phys. Rev. A **6**, 764 (1972).
[4]C. Yamanaka, T. Yamanaka, T. Sasaki, K. Yoshida, M. Waki, and H. B. Kang, Phys. Rev. A **6**, 2335 (1972).
[5]G. H. McCall, F. Young, A. W. Ehler, J. F. Kephart, and R. P. Godwin, Phys. Rev. Lett. **30**, 1116 (1973).
[6]G. Basov, Yu. S. Ivanov, O. N. Krokhin, Yu. A. Mikhailov, G. V. Sklizkov, and S. I. Fedotov, JETP Lett. **15**, 417 (1972).
[7]J. Lindl, Phys. Plasmas **2**, 3933 (1995).
[8]O. A. Hurricane, D. A. Callahan, D. T. Casey, E. L. Dewald, T. R. Dittrich, T. Döppner, M. A. Barrios Garcia, D. E. Hinkel, L. F. Berzak Hopkins, P. Kervin, J. L. Kline, S. Le Pape, T. Ma, A. G. MacPhee, J. L. Milovich, J. Moody, A. E. Pak, P. K. Patel, H.-S. Park, B. A. Remington, H. F. Robey, J. D. Salmonson, P. T. Springer, R. Tommasini, L. R. Benedetti, J. A. Caggiano, P. Celliers, C. Cerjan, R. Dylla-Spears, D. Edgell, M. J. Edwards, D. Fittinghoff, G. P. Grim, N. Guler, N. Izumi, J. A. Frenje, M. Gatu Johnson, S. Haan, R. Hatarik, H. Herrmann, S. Khan, J. Knauer, B. J. Kozioziemski, A. L. Kritcher, G. Kyrala, S. A. Maclaren, F. E. Merrill, P. Michel, J. Ralph, J. S. Ross, J. R. Rygg, M. B. Schneider, B. K. Spears, K. Widmann, and C. B. Yeamans, Phys. Plasmas **21**, 056314 (2014).
[9]P. A. Norreys, A. P. Fews, F. N. Beg, A. R. Bell, A. E. Dangor, P. Lee, M. B. Nelson, H. Schmidt, M. Tatarakis, and M. D. Cable, Plasma Phys. Controlled Fusion **40**, 175–182 (1998).
[10]M. H. Key, M. D. Cable, T. E. Cowan, K. G. Estabrook, B. A. Hammel, S. P. Hatchett, E. A. Henry, D. E. Hinkel, J. D. Kilkenny, J. A. Koch, W. L. Kruer, A. B. Langdon, B. F. Lasinski, R. W. Lee, B. J. MacGowan, A. MacKinnon, J. D. Moody, M. J. Moran, A. A. Offenberger, D. M. Pennington, M. D. Perry, T. J. Phillips, T. C. Sangster, M. S. Singh, M. A. Stoyer, M. Tabak, G. L. Tietbohl, M. Tsukamoto, K. Wharton, and S. C. Wilks, Phys. Plasmas **5**, 1966 (1998).
[11]L. Disdier, J.-P. Garconnet, G. Malka, and J.-L. Miquel, Phys. Rev. Lett. **82**, 1454 (1999).
[12]K. A. Tanaka, R. Kodama, H. Fujita, M. Heya, N. Izumi, Y. Kato, Y. Kitagawa, K. Mima, N. Miyanaga, T. Norimatsu, A. Pukhov, A. Sunahara, K. Takahashi, M. Allen, H. Habara, T. Iwatani, T. Matusita, T. Miyakosi, M. Mori, H. Setoguchi, T. Sonomoto, M. Tanpo, S. Tohyama, H. Azuma, T. Kawasaki, T. Komeno, O. Maekawa, S. Matsuo, T. Shozaki, Ka. Suzuki, H. Yoshida, T. Yamanaka, Y. Sentoku, F. Weber, T. W. Barbee, Jr., and L. DaSilva, Phys. Plasmas **7**, 2014 (2000).
[13]G. Pretzler, A. Saemann, A. Pukhov, D. Rudolph, T. Schätz, U. Schramm, P. Thirolf, D. Habs, K. Eidmann, G. D. Tsakiris, J. Meyer-ter-Vehn, and K. J. Witte, Phys. Rev. E **58**, 1165 (1998).
[14]D. Hilscher, O. Berndt, M. Enke, U. Jahnke, P. V. Nickles, H. Ruhl, and W. Sandner, Phys. Rev. E **64**, 016414 (2001).
[15]S. Karsch, S. Dusterer, H. Schwoerer, F. Ewald, D. Habs, M. Hegelich, G. Pretzler, A. Pukhov, K. Witte, and R. Sauerbrey, Phys. Rev. Lett. **91**, 015001 (2003).
[16]S. Ter-Avetisyan, M. Schnurer, D. Hilscher, U. Jahnke, S. Busch, P. V. Nickles, and W. Sandner, Phys. Plasmas **12**, 012702 (2005).
[17]T. Ditmire, J. Zweiback, V. P. Yanovsky, T. E. Cowan, G. Hays, and K. B. Wharton, Nature **398**, 489–492 (1999).
[18]T. Ditmire, J. Zweiback, V. P. Yanovsky, T. E. Cowan, G. Hays, and K. B. Wharton, Phys. Plasmas **7**, 1993 (2000).
[19]J. Zweiback, T. E. Cowan, J. H. Hartley, R. Howell, K. B. Wharton, J. K. Crane, V. P. Yanovsky, G. Hays, R. A. Smith, and T. Ditmire, Phys. Plasmas **9**, 3108 (2002).
[20]G. Grillon, Ph. Balcou, J.-P. Chambaret, D. Hulin, J. Martino, S. Moustaizis, L. Notebaert, M. Pittman, Th. Pussieux, A. Rousse, J.-Ph. Rousseau, S. Sebban, O. Sublemontier, and M. Schmidt, Phys. Rev. Lett. **89**, 065005 (2002).
[21]S. P. Hatchett, C. G. Brown, T. E. Cowan, E. A. Henry, J. S. Johnson, M. H. Key, J. A. Koch, A. B. Langdon, B. F. Lasinski, R. W. Lee, A. J. Mackinnon, D. M. Pennington, M. D. Perry, T. W. Phillips, M. Roth, T. C. Sangster, M. S. Singh, R. A. Snavely, M. A. Stoyer, S. C. Wilks, and K. Yasuike, Phys. Plasmas **7**, 2076 (2000).
[22]S. C. Wilks, A. B. Langdon, T. E. Cowan, M. Roth, M. Singh, S. Hatchett, M. H. Key, D. Pennington, A. MacKinnon, and R. A. Snavely, Phys. Plasmas **8**, 542 (2001).
[23]L. Willingale, G. M. Petrov, A. Maksimchuk, J. Davis, R. R. Freeman, A. S. Joglekar, T. Matsuoka, C. D. Murphy, V. M. Ovchinnikov, A. G. R. Thomas, L. Van Woerkom, and K. Krushelnick, Phys. Plasmas **18**, 083106 (2011).
[24]K. L. Lancaster, S. Karsch, H. Habara, F. N. Beg, E. L. Clark, R. Freeman, M. H. Key, J. A. King, R. Kodama, K. Krushelnick, K. W. D. Ledingham, P. McKenna, C. D. Murphy, P. A. Norreys, R. Stephens, C. Stoeckl, Y. Toyama, M. S. Wei, and M. Zepf, Phys. Plasmas **11**, 3404 (2004).
[25]D. P. Higginson, J. M. McNaney, D. C. Swift, G. M. Petrov, J. Davis, J. A. Frenje, L. C. Jarrott, R. Kodama, K. L. Lancaster, A. J. Mackinnon, H. Nakamura, P. K. Patel, G. Tynan, and F. N. Beg, Phys. Plasmas **18**, 100703 (2011).
[26]C. Zulick, F. Dollar, V. Chvykov, J. Davis, G. Kalinchenko, A. Maksimchuk, G. M. Petrov, A. Raymond, A. G. R. Thomas, L. Willingale, V. Yanovsky, and K. Krushelnick, Appl. Phys. Lett. **102**, 124101 (2013).
[27]M. Roth, D. Jung, K. Falk, N. Guler, O. Deppert, M. Devlin, A. Favalli, J. Fernandez, D. Gautier, M. Geissel, R. Haight, C. E. Hamilton, B. M. Hegelich, R. P. Johnson, F. Merrill, G. Schaumann, K. Schoenberg, M. Schollmeier, T. Shimada, T. Taddeucci, J. L. Tybo, F. Wagner, S. A. Wender, C. H. Wilde, and G. A. Wurden, Phys. Rev. Lett. **110**, 044802 (2013).
[28]T. Esirkepov, M. Borghesi, S. V. Bulanov, G. Mourou, and T. Tajima, Phys. Rev. Lett. **92**, 175003 (2004).
[29]H. Daido, M. Yamanaka, K. Mima, K. Nishihara, S. Nakai, Y. Kitagawa, E. Miura, C. Yamanaka, and A. Hasegawa, Appl. Phys. Lett. **51**, 2195 (1987).
[30]W. Bang, G. Dyer, H. J. Quevedo, A. C. Bernstein, E. Gaul, M. Donovan, and T. Ditmire, Phys. Rev. E **87**, 023106 (2013).
[31]V. S. Belyaev, V. I. Vinogradov, A. S. Kurilov, A. P. Matafonov, V. P. Andrianov, G. N. Ignat'ev, A. Ya. Faenov, T. A. Pikuz, I. Yu. Skobelev, A. I. Magunov, S. A. Pikuz, Jr., and B. Yu. Sharkov, J. Exp. Theor. Phys. **98**, 1133–1137 (2004).
[32]V. S. Belyaev, V. I. Vinogradov, A. P. Matafonov, V. P. Krainov, V. S. Lisitsa, V. P. Andrianov, and G. N. Ignatyev, Laser Phys. **16**, 1647 (2006).
[33]A. V. Bessarab, V. A. Gaidash, G. V. Dolgoleva, N. V. Zhidkov, V. M. Izgorodin, G. A. Kirillov, G. G. Kochemasov, A. V. Kunin, D. N. Litvin, V. M. Murugov, G. F. Nasyrov, V. T. Punin, V. G. Rogachev, A. V. Senik, N. A. Suslov, G. V. Tachaev, and V. I. Shemyakin, Sov. Phys. JETP **75**, 970 (1992).
[34]S. Fritzler, Z. Najmudin, V. Malka, K. Krushelnick, C. Marle, B. Walton, M. S. Wei, R. J. Clarke, and A. E. Dangor, Phys. Rev. Lett. **89**, 165004 (2002).
[35]H. Habara, K. L. Lancaster, S. Karsch, C. D. Murphy, P. A. Norreys, R. G. Evans, M. Borghesi, L. Romagnani, M. Zepf, T. Norimatsu, Y. Toyama, R. Kodama, J. A. King, R. Snavely, K. Akli, B. Zhang, R. Freeman, S. Hatchett, A. J. MacKinnon, P. Patel, M. H. Key, C. Stoeckl, R. B. Stephens, R. A. Fonseca, and L. O. Silva, Phys. Rev. E **70**, 046414 (2004).
[36]H. Habara, R. Kodama, Y. Sentoku, N. Izumi, Y. Kitagawa, K. A. Tanaka, K. Mima, and T. Yamanaka, Phys. Rev. E **69**, 036407 (2004).

[37]H. Zhang, H. Lu, S. Li, Y. Xu, X. Guo, Y. Leng, J. Liu, B. Shen, R. Li, and Z. Xu, Appl. Phys. Express **7**, 026401 (2014).
[38]N. Izumi, Y. Sentoku, H. Habara, K. Takahashi, F. Ohtani, T. Sonomoto, R. Kodama, T. Norimatsu, H. Fujita, Y. Kitagawa, K. Mima, K. A. Tanaka, and T. Yamanaka, Phys. Rev. E **65**, 036413 (2002).
[39]S. Karsch, Ph.D. thesis, Ludwig-Maximilians-Universitat Munchen, 2002.
[40]O. Komeda, Y. Nishimura, Y. Mori, R. Hanayama, K. Ishii, S. Nakayama, Y. Kitagawa, T. Sekine, N. Sato, T. Kurita, T. Kawashima, H. Kan, N. Nakamura, T. Kondo, M. Fujine, H. Azuma, T. Motohiro, T. Hioki, M. Kakeno, A. Sunahara, Y. Sentoku, and E. Miura, Nat. Sci. Rep. **3**, 2561 (2013).
[41]S. Lee, S. Park, K. Yea, D. Kwon, S. Park, Y. Jeong, and H. Cha, J. Korean Phys. Soc. **55**, 543 (2009).
[42]H. Y. Lu, J. S. Liu, C. Wang, W. T. Wang, Z. L. Zhou, A. H. Deng, C. Q. Xia, Y. Xu, X. M. Lu, Y. H. Jiang, Y. X. Leng, X. Y. Liang, G. Q. Ni, R. X. Li, and Z. Z. Xu, Phys. Rev. A **80**, 051201 (2009).
[43]K. W. Madison, P. K. Patel, M. Allen, D. Price, and T. Ditmire, J. Opt. Soc. Am. B **20**, 113 (2003).
[44]K. W. Madison, P. K. Patel, M. Allen, D. Price, R. Fitzpatrick, and T. Ditmire, Phys. Rev. A **70**, 053201 (2004).
[45]S. Nam, J. Han, Y. Rhee, Y. Cha, Y. Lee, J. Mun, S. Lee, S. Kwon, and H. Cha, J. Korean Phys. Soc. **56**, 295 (2010).
[46]P. A. Norreys, K. L. Lancaster, H. Habara, J. R. Davies, J. T. Mendonça, R. J. Clarke, B. Dromey, A. Gopal, S. Karsch, R. Kodama, K. Krushelnick, S. D. Moustaizis, C. Stoeckl, M. Tatarakis, M. Tampo, N. Vakakis, M. S. Wei, and M. Zepf, Plasma Phys. Controlled Fusion **47**, L49–L56 (2005).
[47]A. Youssef, R. Kodama, H. Habara, K. A. Tanaka, Y. Sentoku, M. Tampo, and Y. Toyama, Phys. Plasmas **12**, 110703 (2005).
[48]J. Krasa, D. Klir, A. Velyhan, D. Margarone, E. Krouský, K. Jungwirth, J. Skala, M. Pfeifer, J. Kravarik, P. Kubes, K. Rezac, and J. Ullschmied, Laser Part. Beams **31**, 395 (2013).
[49]T. H. Tan, G. H. McCall, and A. H. Williams, Phys. Fluids **27**, 296–301 (1984).
[50]S. J. Gitomer, R. D. Jones, F. Begay, A. W. Ehler, J. F. Kephart, and R. Kristal, Phys. Fluids **29**, 2679 (1986).
[51]D. C. Brown, IEEE J. Quantum Electron. **33**, 861–873 (1997).
[52]D. Batani, S. Baton, A. Casner, S. Depierreux, M. Hohenberger, O. Klimo, M. Koenig, C. Labaune, X. Ribeyre, C. Rousseaux, G. Schurtz, W. Theobald, and V. T. Tikhonchuk, Nucl. Fusion **54**, 054009 (2014).
[53]K. Jungwirth, A. Cejnarova, L. Juha, B. Kralikova, J. Krasa, E. Krousky, P. Krupickova, L. Laska, K. Masek, T. Mocek, M. Pfeifer, A. Präg, O. Renner, K. Rohlena, B. Rus, J. Skala, P. Straka, and J. Ullschmied, Phys. Plasmas **8**, 2495 (2001).
[54]J. Krasa, D. Margarone, D. Klir, A. Velyhan, A. Picciotto, E. Krousky, K. Jungwirth, J. Skala, M. Pfeifer, J. Ullschmied, J. Kravarik, K. Rezac, P. Kubes, P. Parys, and L. Ryc, IEEE Trans. Plasma Sci. **41**, 2819–2824 (2013).
[55]K. Rezac, D. Klir, P. Kubes, and J. Kravarik, Plasma Phys. Controlled Fusion **54**, 105011 (2012).
[56]J. Krasa, P. Parys, L. Velardi, A. Velyhan, L. Ryc, D. Delle Sise, and V. Nassisi, Laser Part. Beams **32**, 15–20 (2014).
[57]D. Margarone, J. Krasa, L. Giuffrida, A. Picciotto, L. Torrisi, T. Nowak, P. Musumeci, A. Velyhan, J. Prokupek, L. Laska, T. Mocek, J. Ullschmied, and B. Rus, J. Appl. Phys. **109**, 103302 (2011).
[58]G. A. P. Cirrone, A. Tramontana, G. Candiano, M. Carpinelli, S. Cavallaro, M. Cutroneo, G. Cutton, C. De Martinis, D. Giove, J. Krasa, G. Korn, M. Maggiore, D. Margarone, P. Pisciotta, J. Prokupek, F. Romano, F. Schillaci, V. Scuderi, L. Torrisi, and A. Velyhan, JINST **9**, T08001 (2014).
[59]H. Ing, R. A. Noulty, and T. D. McLean, Radiat. Meas. **27**, 1 (1997).
[60]D. Klir, J. Kravarik, P. Kubes, K. Rezac, E. Litseva, K. Tomaszewski, L. Karpinski, M. Paduch, and M. Scholz, Rev. Sci. Instrum. **82**, 033505 (2011).
[61]T. Goorley, M. James, T. Booth, F. Brown, J. Bull, L. J. Cox, J. Durkee, J. Elson, M. Fensin, R. A. Forster, J. Hendricks, H. G. Hughes, R. Johns, B. Kiedrowski, R. Martz, S. Mashnik, G. McKinney, D. Pelowitz, R. Prael, J. Sweezy, L. Waters, T. Wilcox, and T. Zukaitis, Nucl. Technol. **180**, 298–315 (2012).
[62]A. Youssef and R. Kodama, Nucl. Fusion **50**, 035010 (2010).
[63]A. Youssef, Phys. Scr. **87**, 015501 (2013).
[64]R. H. Siemssen, M. Cosack, and R. Felst, Nucl. Phys. **69**, 209–226 (1965).
[65]H. Fuchs, K. Grabisch, P. Kraaz, and G. Roscher, Nucl. Phys. **A105**, 590–600 (1967).
[66]J. Krasa, D. Klir, A. Velyhan, E. Krousky, M. Pfeifer, K. Rezac, J. Cikhardt, K. Turek, J. Ullschmied, and K. Jungwirth, High Power Laser Sci. Eng. **2**, e19 (2014).
[67]M. B. Chadwick, P. Oblozinsky, M. Herman, M. Herman, N. M. Greene, R. D. McKnight, D. L. Smith, P. G. Young, R. E. Macfarlane, G. M. Hale, S. C. Frankle, A. C. Kahler, T. Kawano, R. C. Little, D. G. Madland, P. Moller, R. D. Mosteller, P. R. Page, P. Talou, H. Trellue, M. C. White, W. B. Wilson, R. Arcilla, C. L. Dunford, S. F. Mughabghab, B. Pritychenko, D. Rochman, A. A. Sonzogni, C. R. Lubitz, T. H. Trumbull, J. P. Weinman, D. A. Brown, D. E. Cullen, D. P. Heinrichs, D. P. McNabb, H. Derrien, M. E. Dunn, N. M. Larson, L. C. Leal, A. D. Carlson, R. C. Block, J. B. Briggs, E. T. Cheng, H. C. Huria, M. L. Zerkle, K. S. Kozier, A. Courcelle, V. Pronyaev, and S. C. van der Marck, Nucl. Data Sheets **107**, 2931 (2006).
[68]D. T. L. Jones and C. M. Bartle, Nucl. Instrum. Methods **118**, 525–529 (1974).
[69]J. F. Ziegler, Nucl. Instrum. Methods B **219–220**, 1027 (2004).
[70]F. C. Young, J. Golden, and C. A. Kapetanakos, Rev. Sci. Instrum. **48**, 432 (1977).
[71]D. R. Harding, T. C. Sangster, D. D. Meyerhofer, P. W. McKenty, L. D. Lund, L. Elasky, M. D. Wittman, W. Seka, S. J. Loucks, R. Janezic, T. H. Hinterman, D. H. Edgell, D. Jacobs-Perkins, and R. Q. Gram, Fusion Sci. Technol. **48**, 1299–1306 (2005).
[72]D. Klir, A. V. Shishlov, V. A. Kokshenev, P. Kubes, A. Yu. Labetsky, K. Rezac, R. K. Cherdizov, J. Cikhardt, B. Cikhardtova, G. N. Dudkin, F. I. Fursov, A. A. Garapatsky, B. M. Kovalchuk, J. Kravarik, N. E. Kurmaev, H. Orcikova, V. N. Padalko, N. A. Ratakhin, O. Sila, K. Turek, and V. A. Varlachev, Plasma Phys. Controlled Fusion **54**, 044005 (2015).
[73]D. Klir, P. Kubes, K. Rezac, J. Cikhardt, J. Kravarik, O. Sila, A. V. Shishlov, B. M. Kovalchuk, N. A. Ratakhin, V. A. Kokshenev, A. Yu. Labetsky, R. K. Cherdizov, F. I. Fursov, N. E. Kurmaev, G. N. Dudkin, B. A. Nechaev, V. N. Padalko, H. Orcikova, and K. Turek, Phys. Rev. Lett. **112**, 095001 (2014).
[74]C. A. Coverdale, C. Deeney, A. L. Velikovich, R. W. Clark, Y. K. Chong, J. Davis, J. Chittenden, C. L. Ruiz, G. W. Cooper, A. J. Nelson, J. Franklin, P. D. LePell, J. P. Apruzese, J. Levine, J. Banister, and N. Qi, Phys. Plasmas **14**, 022706 (2007).
[75]J. Denavit, Phys. Rev. Lett. **69**, 3052 (1992).
[76]S. C. Wilks, W. L. Kruer, M. Tabak, and A. B. Langdon, Phys. Rev. Lett. **69**, 1383 (1992).
[77]E. G. Gamaly, Phys. Fluids **5**, 3765 (1993).